Acta Crystallographica Section B
Structural Science
ISSN 0108-7681

Vacancy-ordering effects in AlB_2-type $ErGe_{2-x}$ ($0.4 < x \leq 0.5$)

Jeppe Christensen,[a]* Sven Lidin,[a] Bernard Malaman[b] and Gerard Venturini[b]

[a]Inorganic Chemistry, Arrhenius Laboratory, Stockholm University, SE-106 91 Stockholm, Sweden, and [b]Laboratoire de Chimie du Solide Minéra, Université de Nancy I, Boîte Postale 239, 54506 Vandoeuvre les Nancy CEDEX, France

Correspondence e-mail: jeppe@inorg.su.se

Received 19 September 2007
Accepted 22 February 2008

In the Er–Ge system, the compostion range $ErGe_2$ to Er_2Ge_3 has been investigated. Eight samples were produced by arc melting of the elements, and analyzed using X-ray powder diffraction. Nine crystal structures were found to be present in the samples. The structures are described as a homologous series and presented within the superspace formalism using the superspace group $X2/m(\alpha 0\gamma)0s$, X representing the centring vector $(\frac{1}{2}, \frac{1}{2}, 0, \frac{1}{2})$. In this description the modulation vector $\mathbf{q} = (\alpha\mathbf{a}^* + \gamma\mathbf{c}^*)$ is shown to be a direct measure of the Ge content as $ErGe_{2-\alpha}$ (α falls in the range $\frac{1}{3}$ to $\frac{1}{2}$). The large composition range is achieved by extended vacancy ordering in the planar 6^3 net of Ge with subsequent relaxation.

1. Introduction

The AlB_2 structure type is present in a vast variety of binary and ternary intermetallic systems. Many derivative structures can also be found (Hoffmann & Pöttgen, 2001). The structural study of compounds with a nominal composition of the form AB_2, A = rare-earth metal and B = Si or Ge, dates back more than 50 years (Zachariasen, 1949; Perri *et al.*, 1959; Mayer *et al.*, 1962; Tharp, 1962), but in the last decade special interest has been directed towards these types of systems owing to their magnetic and electronic properties, and a great amount of work has been involved in these studies (Netzer, 1995; Ijjaali *et al.*, 1999; Venturini *et al.*, 1999*a*; Boulet *et al.*, 2001; Palenzona *et al.*, 2003; Boulet *et al.* 2003). The structures tend

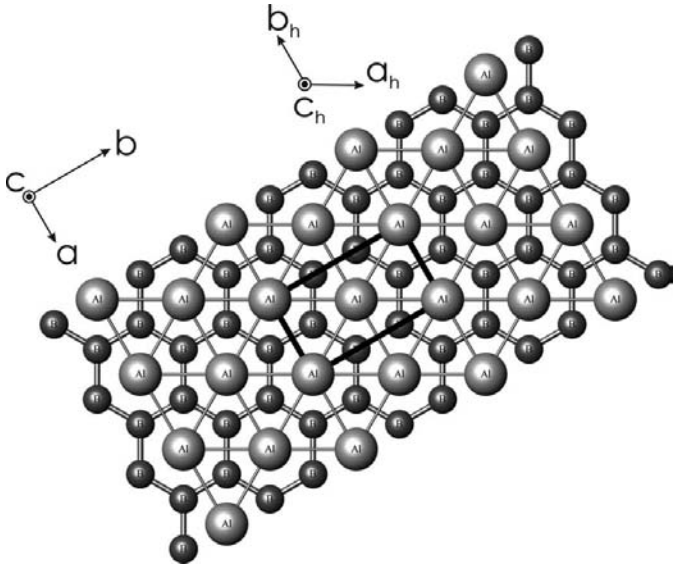

Figure 1
Projection of the AlB_2 structure along the c axis. Al and B atoms are in separate layers. The relation between hexagonal (*P6/mmm*; No. 191) and orthorhombic (*Cmmm*; No. 65) settings is shown.

Table 1
Phase distribution obtained.

Nominal composition	Refined composition	$ErGe_{2-\delta}$	$ErGe_{2-\delta}$ (%)	$ErGe_{1.83}$ (%)	Er_2O_3 (%)
$Er_{39.25}Ge_{60.75}$	$Er_{38.5471}Ge_{61.4529}$	$ErGe_{1.59423\ (18)}$	61.6	34.0	4.4
$Er_{39.50}Ge_{60.50}$	$Er_{38.5521}Ge_{61.4479}$	$ErGe_{1.59389\ (16)}$	70.0	25.4	4.6
$Er_{39.75}Ge_{60.25}$	$Er_{38.5672}Ge_{61.4328}$	$ErGe_{1.59288\ (13)}$	85.6	10.7	3.7
$Er_{40.00}Ge_{60.00}$	$Er_{38.5936}Ge_{61.4064}$	$ErGe_{1.59110\ (17)}$	90.5	5.5	4.0
$Er_{40.25}Ge_{59.75}$	$Er_{38.6823}Ge_{61.3177}$	$ErGe_{1.58516\ (17)}$	95.9	0	4.1
$Er_{40.50}Ge_{59.50}$	$Er_{38.9075}Ge_{61.0925}$	$ErGe_{1.57020\ (16)}$	96.1	0	3.9
$Er_{40.75}Ge_{59.25}$	$Er_{39.0268}Ge_{60.9732}$	$ErGe_{1.56234\ (14)}$	96.5	0	3.5
$Er_{41.00}Ge_{59.00}$	$Er_{39.0451}Ge_{60.9549}$	$ErGe_{1.56114\ (17)}$	81.30	0	3.4
	$Er_{40.0000}Ge_{60.0000}$	$ErGe_{3/2}$	15.3		

Table 2
Unit-cell parameters obtained from the measured diffractograms.

Sample	*a*	*b*	*c*	β	Volume
$ErGe_{1.59423\ (18)}$	3.9208 (2)	6.7547 (4)	4.0945 (2)	89.811 (4)	108.439 (13)
$ErGe_{1.59389\ (16)}$	3.9206 (2)	6.7543 (4)	4.09383 (19)	89.813 (4)	108.409 (13)
$ErGe_{1.59288\ (13)}$	3.92030 (18)	6.7532 (3)	4.09406 (16)	89.813 (3)	108.389 (11)
$ErGe_{1.59110\ (17)}$	3.9198 (2)	6.7518 (4)	4.0941 (2)	89.813 (4)	108.354 (13)
$ErGe_{1.58516\ (17)}$	3.9183 (2)	6.7475 (4)	4.0932 (2)	89.813 (4)	108.217 (13)
$ErGe_{1.57020\ (16)}$	3.9142 (2)	6.7363 (4)	4.0917 (2)	89.810 (4)	107.885 (14)
$ErGe_{1.56234\ (14)}$	3.9117 (2)	6.7296 (3)	4.09129 (19)	89.805 (4)	107.699 (12)
$ErGe_{1.56114\ (17)}$	3.9113 (3)	6.7290 (5)	4.0912 (2)	89.805 (5)	107.674 (16)
$ErGe_{3/2}$	3.8901 (10)	6.6544 (11)	4.0980 (8)	89.74 (2)	106.081 (15)

to be very complicated, but in special cases a good description can be achieved using a normal three-dimensional approach (Smith *et al.*, 1965; Pöttgen *et al.*, 1998; Venturini *et al.*, 1999*b*).

The well known structure of AlB_2 consists of 3^6 layers of Al atoms alternating with planar 6^3 nets of boron. This can be described either using the standard hexagonal setting with the space group *P*6/*mmm* (No. 191) or the orthorhombic setting with space group *Cmmm* (No. 65). The relation between the two cells is shown in Fig. 1. If there is a small axial shift in the way the layers are stacked, the symmetry becomes monoclinic *C*2/*m* (No. 12).

When Venturini *et al.* (1999*a*) began investigations of rare-earth germanides they observed powder diffraction patterns showing both orthorhombic and monoclinic splitting of the basic AlB_2 lines. Additionally they also observed satellite reflections with a position varying with composition.

The aim of the present work is to provide a comprehensive (3 + 1)-dimensional model for this type of vacancy-ordered AlB_2 structure, and to use this model to refine commensurably and incommensurably modulated members of this family.

2. Experimental

Compounds of $ErGe_{2-\delta}$ were synthesized in the range $Er_{41}Ge_{59}$ to $Er_{39.25}Ge_{60.75}$ in steps of 0.25 at % Ge. Stoichiometric mixtures of the elements were arc-melted and subsequently annealed to obtain equilibrium. The samples were powdered and PXRD (powder X-ray diffraction) data were collected using a capillary in transmission mode. All measurements were carried out on an X'pert PRO diffractometer using Cu $K\alpha$ radiation with the wavelengths $\lambda_{K\alpha1}$ = 1.54056 and $\lambda_{K\alpha2}$ = 1.54439 and the intensity ratio 2:1. Data were acquired by continuous measurements in the 2θ range 8.51736–129.99157° with a step size of 0.01671°, giving a total number of 7270 unique measuring points. The number of identified reflections for the target compound for each experiment is presented in §5. The Rietveld refinements were carried out using the software package *JANA*2000 (Petricek *et al.*, 2000). A background correction was achieved using Legendre polynomials to the tenth degree and profile shapes were modelled using pseudo-Voigt functions. The values for the parameters determining these functions, as well as the number of refined parameters, are given in the supplementary material.[1]

The phases resulting from the different synthesis mixtures are shown in Table 1; the refined phase volumes are also given. The corresponding unit cells are given in Table 2. The powder diffractogram from a representative sample is presented in Fig. 2 and the remaining diffractograms can be found in the supplementary material.

The measured diffractograms confirm the previously reported observations of composition-dependent satellites and line-splitting, owing to the orthorhombic and monoclinic distortion of the basic hexagonal AlB_2 lattice. Examples of these observations are given in Fig. 3.

3. Superspace-group determination

In order to describe the entire homologous series a symmetry description that is consistent with all the experimental observations is needed.

As the symmetry of the fully occupied compounds is *P*6/*mmm* (No. 191), the possible choices are either a hexagonal (3 + 2)-dimensional superspace group with two **q** vectors ($\alpha0\gamma$) and ($0\beta\gamma$), or a (3 + 1)-dimensional superspace group with lower symmetry. As no cross-term indexed satellites indicative of a (3 + 2)-dimensional superspace group are observed, a simpler model in a (3 + 1)-dimensional superspace group is a natural first choice. With this choice the **q** vector must be given as ($\alpha0\gamma$) and is not reducible to an axial form. This determines the (3 + 1)-dimensional space group to be monoclinic. The maximal three-dimensional subgroup is given by the sequence

$$P6/mmm \rightarrow Cmmm \rightarrow C12/m1.$$

[1] Supplementary data for this paper are available from the IUCr electronic archives (Reference: CK5030). Services for accessing these data are described at the back of the journal.

Table 3
The initial model describing the fully occupied AlB_2 structure type in the (3 + 1)-dimensional approach.

a	*b*	*c*	*β*
3.009	5.2117	3.262	90

Atom	*x*	*y*	*z*
Er	0	0	0
Ge	0.5	0.1667	0.5

Ge Occ. crenel	Δ	X_4^0
	1	0.25

From the experimental data it is seen that first-order satellites are only observed for reflections systematically absent owing to the C-centring, whereas second-order satellites are only observed for main reflections allowed by the C-centring. That is, for a reflection $hklm$: $h + k + m = 2n$. This is the equivalent of a centring vector $\frac{1}{2}\ \frac{1}{2}\ 0\ \frac{1}{2}$ of the (3 + 1)-dimensional superspace lattice. The allowed superspace groups are then

$$X2/m(\alpha 0\gamma)0s$$
$$X2/m(\alpha 0\gamma)00.$$

The $X2/m(\alpha 0\gamma)0s$ group fulfils the same extinction conditions as $X2/m(\alpha 0\gamma)00$, but in addition contains the extinction condition for the *s*-glide, $h0lm$: $m = 2n$. This latter condition is strictly adhered to in all the cases studied. This determines the superspace group to be $X2/m(\alpha 0\gamma)0s$. The non-standard *X*-centring is used as the standard choice leads to an equivalent, but longer modulation vector. Moreover, the simple relationship between the **q** vector and composition would be lost with the standard setting.

4. Refinement

All samples contain one or more impurity phases. The phase volumes and the unit-cell parameters for these were allowed to refine, but the atomic coordinates and displacement parameters were fixed according to the values in the supplementary material. In the $ErGe_{2-\delta}$ system, there are actually two phases with the composition $ErGe_{1.83} = Er_3Ge_5$. One of these is a hexagonal superstructure of the AlB_2 type structure (discussed in §6), the other belongs to a different structure type not closely related to AlB_2. It is the latter of these phases that is present in our samples.

The model used to describe the main phase is the AlB_2 structure type in monoclinic (3 + 1)-dimensional setting as given in Table 3. We have applied a crenel function for the Ge occupancy to model the partial occupancy in the average three-dimensional structure, and two sinusoidal modulation functions for the Ge position to model the resulting relaxations. The rare-earth position is also modulated using a sinusoidal function. In the structures the modulation corresponds to a relaxation, with atoms moving towards the vacancies. This is illustrated in Fig. 4. The final parameter values after refinement are given in Tables 4 and 5.

As evident from Tables 4 and 5, the refinable parameters do not vary much with α. To stabilize the refinement of the $ErGe_{3/2}$ phase, this information was used to set all the structural parameters except the Ge occupancy equal to the corresponding parameters for the $ErGe_{1.56114}$ phase. The $ErGe_{3/2}$ phase is listed in the tables as it is a *bona fide* member of the structural family.

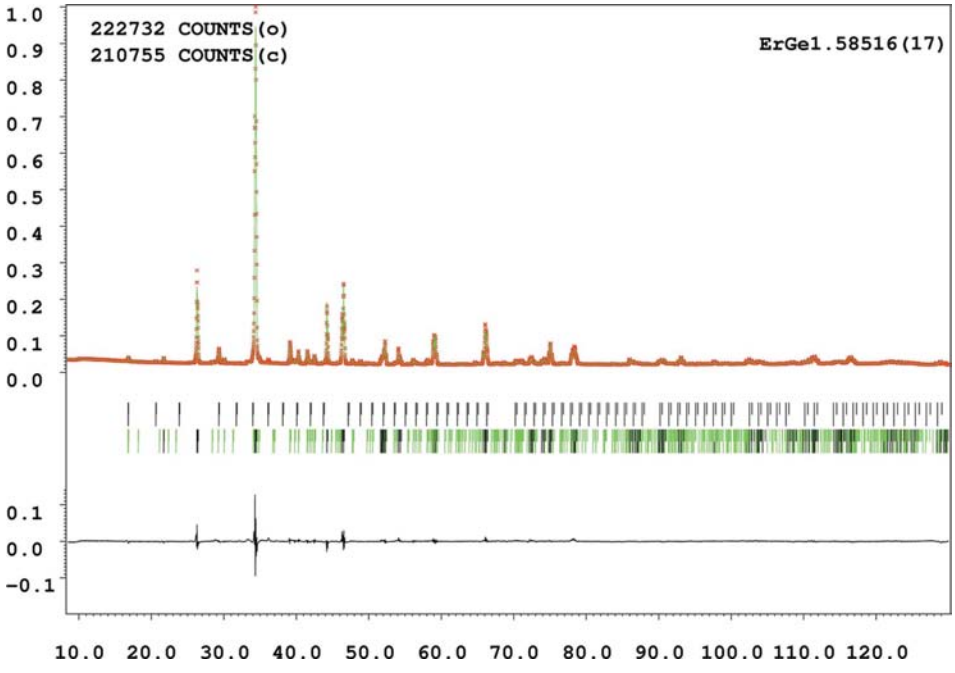

Figure 2
The powder diffractogram from $ErGe_{1.58516\,(7)}$. Red crosses indicate observed data, the green line is the calculated profile, and at the bottom is the difference curve. The tick marks indicate in order from top and downwards: Er_2O_3 and $ErGe_{2-\delta}$. Black tick marks are main reflections and green tick marks indicate satellite positions.

5. Results and discussion

Observations show α to vary more strongly with composition than γ does. This is a result of α relating directly to vacancy ordering within the hexagonal network, whereas γ relates to the secondary effect of stacking of the net planes. To establish the relationship between the **q** vector and the composition, refinements were performed allowing both to vary freely. The result is

Table 4
The final results for the refinable parameters.

Sample	α	γ	Ge Occ. crenel Δ	y (Ge)	Ge U_{iso}	Er U_{iso}
$ErGe_{1.59423\ (18)}$	0.40577 (18)	0.2206 (3)	0.797127 (9)	0.180 (3)	0.0149 (19)	0.0069 (11)
$ErGe_{1.59389\ (16)}$	0.40611 (16)	0.2206 (3)	0.796947 (8)	0.181 (2)	0.0122 (18)	0.0066 (10)
$ErGe_{1.59288\ (13)}$	0.40712 (13)	0.22091 (19)	0.796442 (7)	0.181 (2)	0.0151 (17)	0.0080 (10)
$ErGe_{1.59110\ (17)}$	0.40890 (17)	0.2214 (2)	0.795550 (9)	0.182 (3)	0.015 (2)	0.0094 (13)
$ErGe_{1.58516\ (17)}$	0.41484 (17)	0.2236 (2)	0.792585 (9)	0.178 (3)	0.016 (2)	0.0098 (13)
$ErGe_{1.57020\ (16)}$	0.42980 (16)	0.2278 (2)	0.785097 (8)	0.176 (4)	0.015 (2)	0.0079 (14)
$ErGe_{1.56234\ (14)}$	0.43766 (14)	0.23005 (19)	0.781170 (7)	0.170 (3)	0.0172 (19)	0.0109 (12)
$ErGe_{1.56114\ (17)}$	0.43886 (17)	0.2302 (2)	0.780567 (9)	0.167 (3)	0.0139 (16)	0.0094 (9)
$ErGe_{3/2}$	1/2	1/4	3/4	0.167 (3)	0.0139 (16)	0.0094 (9)

presented in Fig. 5 where α and γ are plotted as a function of the Ge occupancy, and γ is plotted as a function of α. A least-squares refined linear equation is also given for each.

From the family formula sum $ErGe_{2-\delta}$ one can isolate an expression for the Ge occupancy: Ge Occ. = $(2-\delta)/2$ or $O_{Ge} = -0.5\delta + 1$. This is the same as the experimental relationship between α and the occupancy found in Fig. 5, thus $\delta = \alpha$. It is a well known phenomenon that while the occupation itself certainly is a parameter that is rather weakly coupled to the data, the α parameter is determined with much greater accuracy. In the further refinements the occupancy was fixed to the value of α using the expression derived above. Accordingly, the uncertainty for the occupancy was derived from the uncertainty of α.

For each of the refined structures, a representative part of the vacancy-ordered 6^3 net is shown in Fig. 6. The corresponding Rietveld refinement R values are given in Tables 6 and 7, and the experimental details are summarized in Table 8. The structures are seen to be built from characteristic units packing either periodically or modulated according to the value of α.

To relate α and the compositions, consider the units shown in Fig. 7. The unit to the left contains a single, isolated vacancy

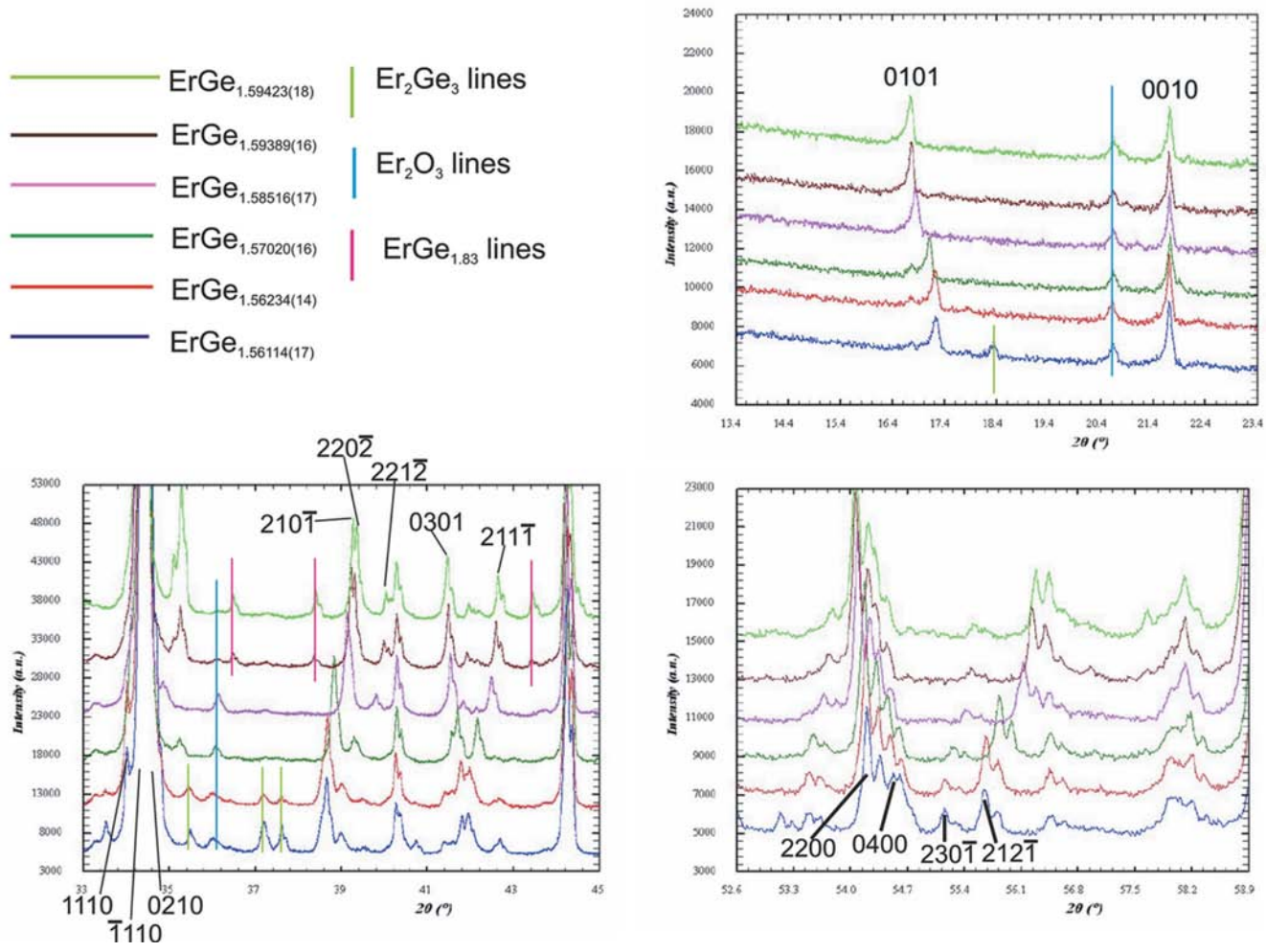

Figure 3
Examples of observed line splitting and satellite positions as a function of composition. The reflections 2200 and 0400 are split owing to the orthorhombic distortion, and 1110 and $\bar{1}110$ are spilt due to a monoclinic distortion. The impurities present are indicated with vertical lines. The data for $ErGe_{1.59288\ (13)}$ and $ErGe_{1.59110\ (17)}$ have been omitted for clarity.

Table 5
The final parameters describing the displacive modulation of the atoms.

Sample	Ge first			Ge second			Er first	Er second	
	A^x_{cos}	A^y_{sin}	A^z_{cos}	A^x_{sin}	A^y_{cos}	A^z_{sin}	A^y_{sin}	A^x_{sin}	A^z_{sin}
$ErGe_{1.59423\ (18)}$	−0.082 (2)	−0.051 (5)	−0.005 (3)	0.054 (4)	0.011 (5)	−0.014 (5)	0.0199 (10)	−0.011 (3)	0.017 (3)
$ErGe_{1.59389\ (16)}$	−0.084 (2)	−0.051 (5)	−0.008 (3)	0.058 (4)	0.010 (4)	−0.017 (5)	0.0206 (9)	−0.010 (3)	0.016 (3)
$ErGe_{1.59288\ (13)}$	−0.0844 (19)	−0.052 (4)	−0.008 (3)	0.053 (4)	0.010 (4)	−0.011 (5)	0.0208 (8)	−0.011 (2)	0.018 (3)
$ErGe_{1.59110\ (17)}$	−0.085 (3)	−0.053 (6)	−0.010 (4)	0.053 (5)	0.010 (5)	−0.011 (6)	0.0217 (11)	−0.012 (3)	0.016 (3)
$ErGe_{1.58516\ (17)}$	−0.082 (3)	−0.048 (6)	−0.009 (4)	0.043 (6)	0.015 (6)	−0.007 (6)	0.0221 (12)	−0.013 (3)	0.019 (3)
$ErGe_{1.57020\ (16)}$	−0.079 (3)	−0.044 (7)	−0.010 (4)	0.044 (6)	0.020 (6)	−0.006 (6)	0.0216 (12)	−0.016 (3)	0.023 (3)
$ErGe_{1.56234\ (14)}$	−0.077 (2)	−0.035 (6)	−0.006 (3)	0.043 (5)	0.027 (5)	−0.003 (5)	0.0204 (11)	−0.016 (3)	0.025 (3)
$ErGe_{1.56114\ (17)}$	−0.079 (2)	−0.032 (6)	−0.008 (3)	0.044 (5)	0.033 (5)	−0.006 (5)	0.0221 (10)	−0.018 (3)	0.030 (2)
$ErGe_{3/2}$	−0.079 (2)	−0.032 (6)	−0.008 (3)	0.044 (5)	0.033 (5)	−0.006 (5)	0.0221 (10)	−0.018 (3)	0.030 (2)

surrounded by three Er atoms. That to the right contains four vacancies surrounded by nine Er atoms. Generally, it is clear that the relation between the number of vacancies, $\square_n$, in a unit, and the number of Er atoms is given by $Er_{2n+1}\square_n$. Similarly, the periphery of the unit consists of six Ge atoms that are shared with two neighbouring units, and $6n$ Ge atoms that are shared with one neighbouring unit, so that the Ge content of the periphery becomes $6/3 + 6n/2 = Ge_{3n+2}$. The overall composition of a unit is thus $Er_{2n+1}Ge_{3n+2}\square_n$. The end structures of the homologous series are given by $n = 0$ and $n = \infty$. The value of n for the observed structures are given in Table 6.

By varying the value of α or n, it is possible to generate any structure in the family. By this approach integer values of n were used to identify the different periodic superstructures, and locate a series of characteristic building units from which the structures are constructed. Some of the units are shown in Fig. 8 and it is seen that they grow ever longer as $n \rightarrow \infty$. The units are shown without relaxation. Any given structure in the

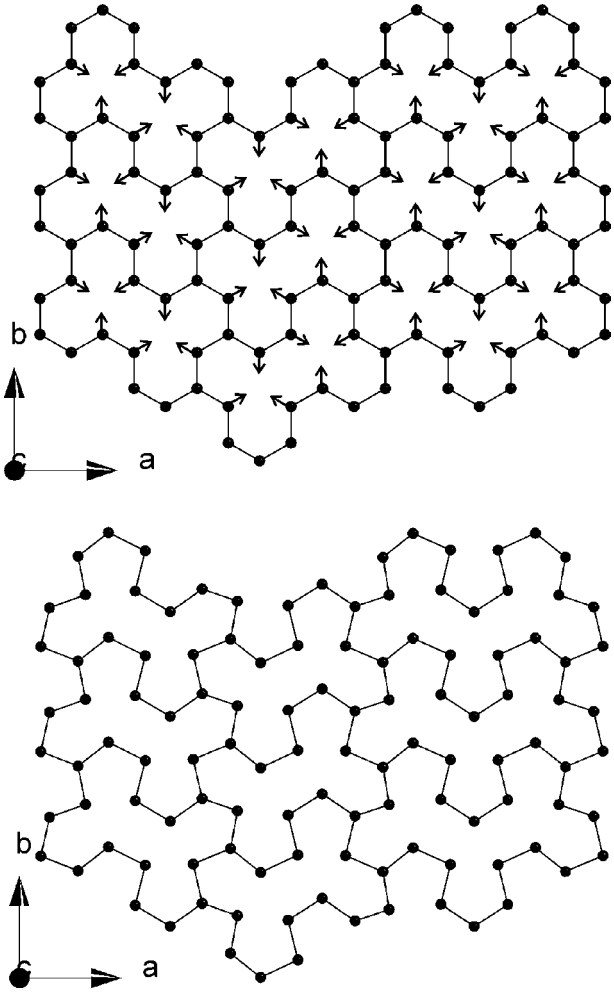

Figure 4
Indication of relaxation in the hexagonal net planes as a result of vacancies. The example used is $ErGe_{1.59423\ (18)}$ before and after refinement.

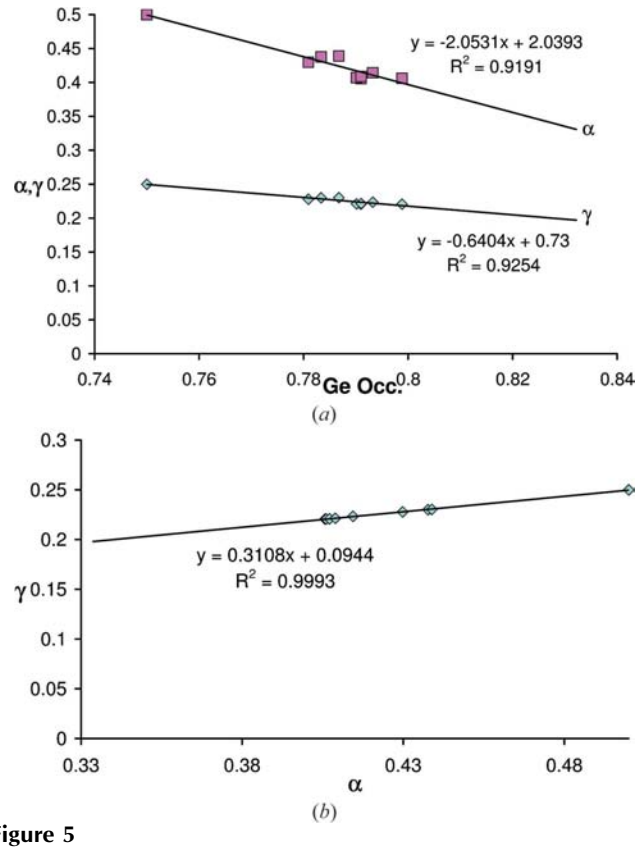

Figure 5
The relation between refined values of α, γ and Ge Occ. Note the very strict linear relation between α and γ.

structural series is built from no more than two different units. When two units are used their difference in the value of n is 1.

In general, n describes the average size of building units in a structure, in terms of vacancies. As such n is not restricted to integer values, but can take on any value between 0 and ∞. From the various expressions for stoichiometry the variation of the structure characteristics as a function of n can be derived. For values of n between 0 and 10, the network occupancy, atomic % and α are shown in Fig. 9. The major changes take place as n goes from 0 to 4.

From previous work (Venturini *et al.*, 1999*a*) information about vacancy ordering in other rare-earth germanides is known. In particular, the authors present in Table 2 refined unit-cell parameters and values for α and γ. By calculating the corresponding value of n for these structures and comparing those to the work presented here, an intriguing pattern arises as illustrated in Fig. 10. Although theoretically possible, not all values of n are observed. Almost all observed structures fall in the interval n = 1.67 to n = 3.6. There is an empty region for values between 0 and 1 arising from relaxations being difficult with these vacancy concentrations. It also seems likely that the 3:5 phase (n = 1) is more favourable than the competing possibilities, giving an empty region for slightly higher values. In the region n = 1.67 to n = 3.6 the vacancy ordering results in structures built from one, or a combination of two, of the

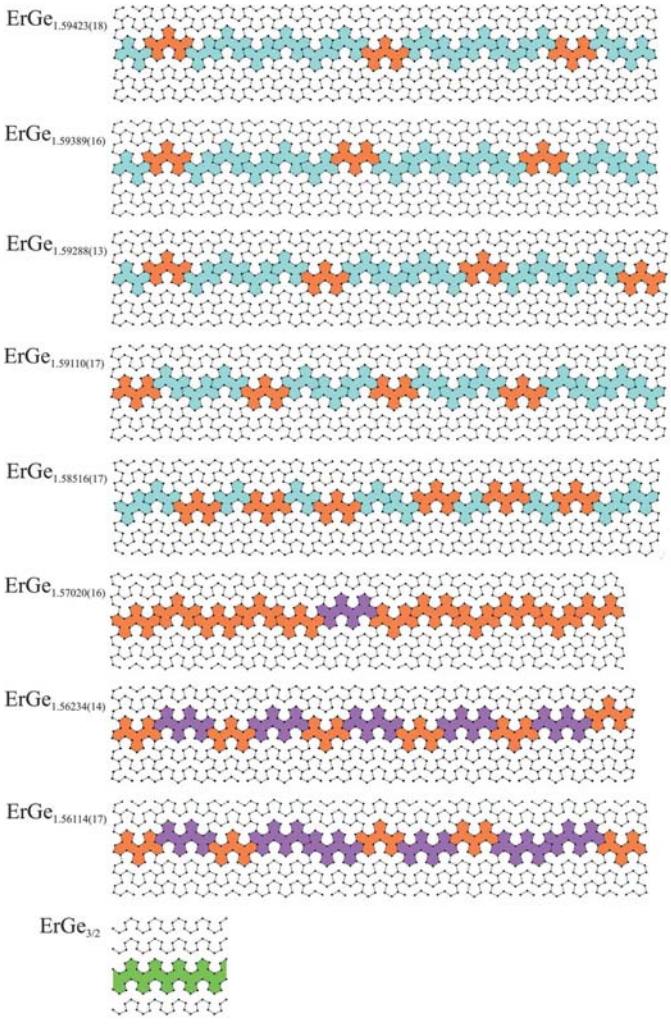

Figure 6
Overview of refined models for the structures investigated. It is seen that the vacancy density increases going from the top and down. Only a single Ge layer is shown for clarity.

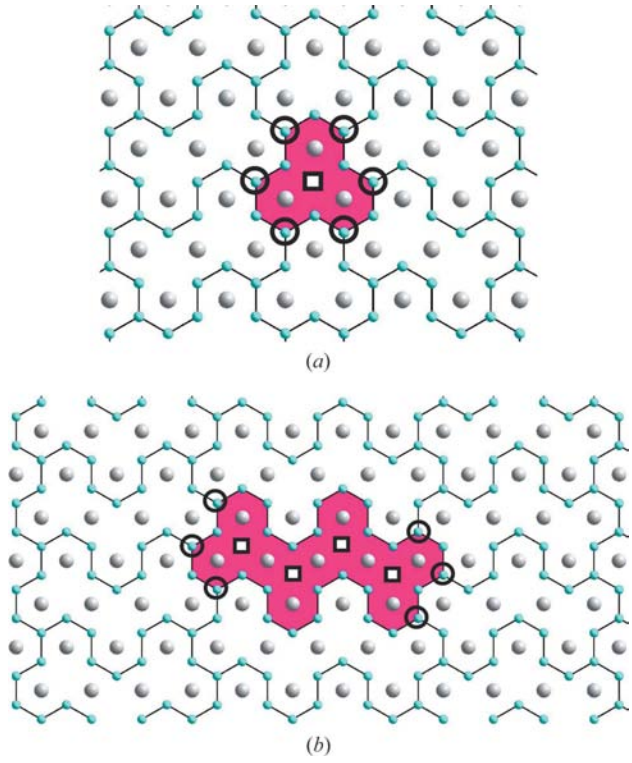

Figure 7
Two examples of the characteristic units building the structures. Vacancies are marked by squares, and the six Ge atoms shared between three units are marked by yellow circles.

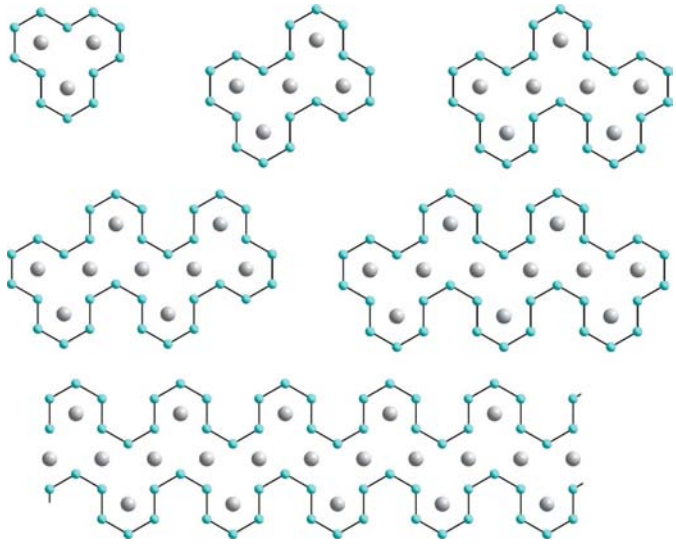

Figure 8
The series of structural building units; from top left it is n = 1, 2, 3, 4, 5, ... ∞ (Fig. 3*b*, Venturini *et al.*, 1999*a*).

Table 6
Summary of the final refinement result for the phases investigated in the present work.

Sample	α	γ	n	ChiQ	R profile
$ErGe_{1.59423\ (18)}$	0.40577 (18)	0.2206 (3)	2.1531	15.88	3.18
$ErGe_{1.59389\ (16)}$	0.40611 (16)	0.2206 (3)	2.1627	14.84	3.08
$ErGe_{1.59288\ (13)}$	0.40712 (13)	0.22091 (19)	2.1916	15.04	3.08
$ErGe_{1.59110\ (17)}$	0.40890 (17)	0.2214 (2)	2.2442	16.05	3.43
$ErGe_{1.58516\ (17)}$	0.41484 (17)	0.2236 (2)	2.4357	17.16	3.57
$ErGe_{1.57020\ (16)}$	0.42980 (16)	0.2278 (2)	3.0613	17.24	3.50
$ErGe_{1.56234\ (14)}$	0.43766 (14)	0.23005 (19)	3.5103	15.72	3.38
$ErGe_{1.56114\ (17)}$	0.43886 (17)	0.2302 (2)	3.5890	14.35	3.26
$ErGe_{3/2}$	1/2	1/4	∞		

Table 7
No. of main satellite reflections used in the refinements and the corresponding resulting R values.

Sample	No. of main	R(all) main	No. of sat. first	R(all) sat. first	No. of sat. second	R(all) sat. second
$ErGe_{1.59423\ (18)}$	91	3.68	145	8.53	177	8.82
$ErGe_{1.59389\ (16)}$	91	3.54	145	7.24	176	8.34
$ErGe_{1.59288\ (13)}$	91	3.01	145	6.81	176	7.30
$ErGe_{1.59110\ (17)}$	107	3.93	164	9.09	202	9.08
$ErGe_{1.58516\ (17)}$	107	3.54	164	8.92	202	10.13
$ErGe_{1.57020\ (16)}$	106	3.38	161	7.99	201	10.92
$ErGe_{1.56234\ (14)}$	105	3.14	161	8.16	202	11.57
$ErGe_{1.56114\ (17)}$	105	3.05	161	8.28	202	10.52
$ErGe_{3/2}$	102	4.05	162	10.00	194	9.98

smaller building units shown in Fig. 8. The selection criteria for the combination of two units is that the value of n should only differ by 1. The empty region from n = 3.6 and upwards is created partly because entropy gained by disordered vacancies is greater than energy gained by ordering, and partly from the 2:3 phase being more stable than more complicated superstructures. This is also supported by the tendency to form a two-phase product for lower germanium content, as seen in the last two synthetic mixtures.

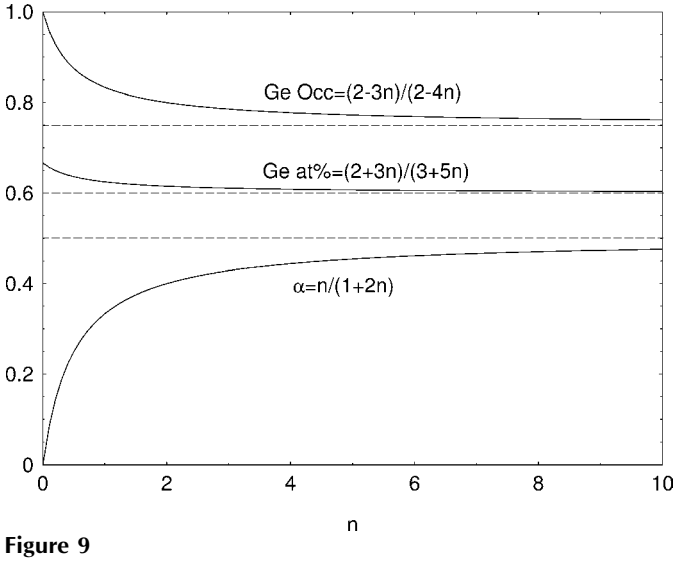

Figure 9
Schematic overview of the structural development as a function of n. The asymptote value for each parameter is indicated by dashed lines.

6. Discussion of the 3:5 phases

The 3:5 phases are part of the homologous series as it is defined here. It is clear though that these phases have very special values for γ that fall outside the linear behaviour otherwise followed. As a result one should expect these structures to be different. The structures can be divided in two groups with γ = 0, space group $P\bar{6}2m$ (No. 189) and γ = 0.5, space group $P\bar{6}2c$ (No. 190). Representative of these structures are the examples Yb_3Ge_5 (Smith *et al.*, 1965) and Y_3Ge_5 (Venturini *et al.*, 1999*b*), respectively. Adjusting the Ge occupancy of our model and entering the values of α and γ generates the structures shown in Figs. 11(*a*) and (*b*). Compared with the observed structures shown in Figs. 11(*c*) and (*d*), it is seen that the model accounts for the structure within the Ge layers, but fails in describing the stacking sequence when γ is outside the linear behaviour otherwise observed. It should be noted that the satellite reflections for the 3:5 phases are often described as being diffuse; this is also the case for Y_3Ge_5. This observation could indicate that the structure is in fact an orthorhombic triple. Further indication of this behaviour can be found in electron-diffraction studies by Arnaud d'Avitaya *et*

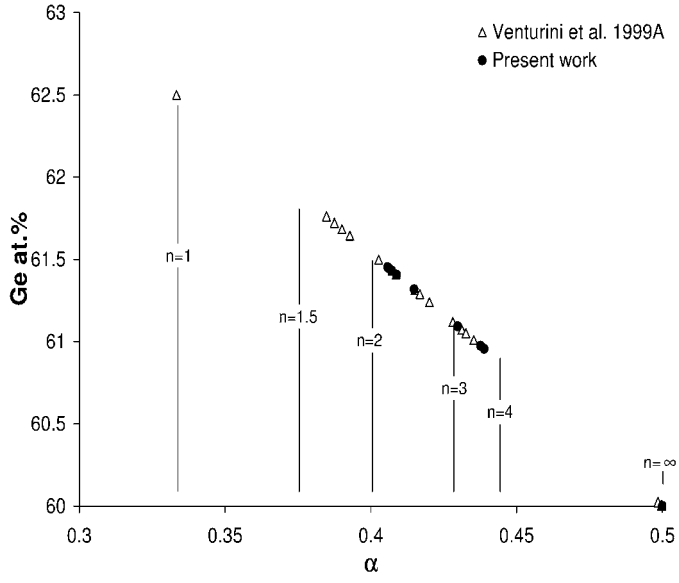

Figure 10
The Ge at. % is related to α through the coupling of the Ge occupancy to α discussed in the beginning of §5. The relation being Ge at. % = $(2-\alpha)/(2-\alpha+1)$. As the synthesis mixtures for the presented phases aimed at, and were evenly distributed in, the range 60–67 at. %, the distribution of observed phases shows that only certain values of n are allowed.

Table 8
Experimental details.

	(I)	(II)	(III)	(IV)	(V)
Crystal data					
Chemical formula	$Er_2Ge_{3.188}$	$Er_2Ge_{3.188}$	$Er_2Ge_{3.186}$	$Er_2Ge_{3.182}$	$Er_2Ge_{3.171}$
M_r	565.9	565.94	565.79	565.50	564.70
Cell setting, space group	Monoclinic, $X2/m(\alpha0\gamma)0s$	Monoclinic, $X2/m(\alpha0\gamma)0s$	Monoclinic, $X2/m(\alpha0\gamma)0s$	Monoclinic, $X2/m(\alpha0\gamma)0s$	Monoclinic, $X2/m(\alpha0\gamma)0s$
Temperature (K)	295	295	295	295	295
a, b, c (Å)	3.9208 (2), 6.7547 (4), 4.0945 (2)	3.9206 (2), 6.7543 (4), 4.09383 (19)	3.92030 (18), 6.7532 (3), 4.09406 (16)	3.9198 (2), 6.7518 (4), 4.0941 (2)	3.9183 (2), 6.7475 (4), 4.0932 (2)
β (°)	89.811 (4)	89.813 (4)	89.813 (3)	89.813 (4)	89.813 (4)
V (Å^3)	108.44 (1)	108.41 (1)	108.39 (1)	108.35 (1)	108.22 (1)
Z	2	2	2	2	2
D_x (Mg m^{-3})	8.664	8.666	8.665	8.664	8.662
Radiation type	Cu $K\alpha$	Cu $K\alpha$	Cu $K\alpha$	Cu $K\alpha$	Cu $K\alpha$
μ (mm^{-1})	91.77	91.79	91.79	91.79	91.83
Specimen form, colour	Cylinder, metallic gray	Cylinder, metallic gray	Cylinder, metallic gray	Cylinder, metallic gray	Cylinder, metallic gray
Data collection					
Diffractometer	PANalytical X'pert PRO	PANalytical X'pert PRO	PANalytical X'pert PRO	PANalytical X'pert PRO	PANalytical X'pert PRO
Data collection method	Specimen mounting: capillary; mode: transmission; scan method: continuous	Specimen mounting: capillary; mode: transmission; scan method: continuous	Specimen mounting: capillary; mode: transmission; scan method: continuous	Specimen mounting: capillary; mode: transmission; scan method: continuous	Specimen mounting: capillary; mode: transmission; scan method: continuous
Absorption correction	Empirical	Empirical	Empirical	Empirical	Empirical
2θ (°)	$2\theta_{min}$ = 13.008, $2\theta_{max}$ = 119.994, increment = 0.017	$2\theta_{min}$ = 13.008, $2\theta_{max}$ = 119.994, increment = 0.017	$2\theta_{min}$ = 13.008, $2\theta_{max}$ = 119.994, increment = 0.017	$2\theta_{min}$ = 8.517, $2\theta_{max}$ = 129.992, increment = 0.017	$2\theta_{min}$ = 8.517, $2\theta_{max}$ = 129.992, increment = 0.017
Refinement					
Refinement on	F^2	F^2	F^2	F^2	F^2
R-factors and goodness-of-fit	R_p = 0.032, R_{wp} = 0.045, R_{exp} = 0.011, S = 3.99	R_p = 0.031, R_{wp} = 0.044, R_{exp} = 0.011, S = 3.85	R_p = 0.031, R_{wp} = 0.045, R_{exp} = 0.012, S = 3.88	R_p = 0.034, R_{wp} = 0.048, R_{exp} = 0.012, S = 4.01	R_p = 0.036, R_{wp} = 0.051, R_{exp} = 0.012, S = 4.14
Excluded region(s)	None	None	None	None	None
Profile function	Pseudo-Voigt	Pseudo-Voigt	Pseudo-Voigt	Pseudo-Voigt	Pseudo-Voigt
No. of parameters	51	51	51	51	41
Weighting scheme	Based on measured s.u.'s	Based on measured s.u.'s	Based on measured s.u.'s	Based on measured s.u.'s	Based on measured s.u.'s
$(\Delta/\sigma)_{max}$	0.050	0.050	0.047	0.416	0.092

	(VI)	(VII)	(VIII)	(IX)
Crystal data				
Chemical formula	$Er_2Ge_{3.14}$	$Er_2Ge_{3.125}$	$Er_2Ge_{3.122}$	Er_2Ge_3
M_r	562.45	561.36	561.15	552.29
Cell setting, space group	Monoclinic, $X2/m(\alpha0\gamma)0s$	Monoclinic, $X2/m(\alpha0\gamma)0s$	Monoclinic, $X2/m(\alpha0\gamma)0s$	Monoclinic, $X2/m(\alpha0\gamma)0s$
Temperature (K)	295	295	295	295
a, b, c (Å)	3.9142 (2), 6.7363 (4), 4.0917 (2)	3.9117 (2), 6.7296 (3), 4.09129 (19)	3.9113 (3), 6.7290 (5), 4.0912 (2)	3.8901 (10), 6.6544 (11), 4.0980 (8)
β (°)	89.810 (4)	89.805 (4)	89.805 (5)	89.74 (2)
V (Å^3)	107.89 (1)	107.70 (1)	107.67 (2)	106.08 (2)
Z	2	2	2	2
D_x (Mg m^{-3})	8.654	8.653	8.651	8.643
Radiation type	Cu $K\alpha$	Cu $K\alpha$	Cu $K\alpha$	Cu $K\alpha$
μ (mm^{-1})	91.87	91.92	91.92	92.35
Specimen form, colour	Cylinder, metallic gray	Cylinder, metallic gray	Cylinder, metallic gray	Cylinder, metallic gray
Data collection				
Diffractometer	PANalytical X'pert PRO	PANalytical X'pert PRO	PANalytical X'pert PRO	PANalytical X'pert PRO
Data collection method	Specimen mounting: capillary; mode: transmission; scan method: continuous	Specimen mounting: capillary; mode: transmission; scan method: continuous	Specimen mounting: capillary; mode: transmission; scan method: continuous	Specimen mounting: capillary; mode: transmission; scan method: continuous
Absorption correction	Empirical	Empirical	Empirical	Empirical
2θ (°)	$2\theta_{min}$ = 8.517, $2\theta_{max}$ = 129.992, increment = 0.017	$2\theta_{min}$ = 8.517, $2\theta_{max}$ = 129.992, increment = 0.017	$2\theta_{min}$ = 8.517, $2\theta_{max}$ = 129.992, increment = 0.017	$2\theta_{min}$ = 8.517, $2\theta_{max}$ = 129.992, increment = 0.017
Refinement				
Refinement on	F^2	F^2	F^2	F^2

Table 8 (continued)

	(VI)	(VII)	(VIII)	(IX)
R factors and goodness-of-fit	R_p = 0.035, R_{wp} = 0.051, R_{exp} = 0.012, S = 4.15	R_p = 0.034, R_{wp} = 0.048, R_{exp} = 0.012, S = 3.97	R_p = 0.033, R_{wp} = 0.046, R_{exp} = 0.012, S = 3.79	R_p = 0.033, R_{wp} = 0.046, R_{exp} = 0.012, S = 3.79
Excluded region(s)	None	None	None	None
Profile function	Pseudo-Voigt	Pseudo-Voigt	Pseudo-Voigt	Pseudo-Voigt
No. of parameters	42	37	36	36
Weighting scheme	Based on measured s.u.'s	Based on measured s.u.'s	Based on measured s.u.'s	Based on measured s.u.'s
$(\Delta/\sigma)_{max}$	0.050	0.046	0.049	0.049

Computer programs used: *JANA*2000 (Petricek *et al.*, 2000).

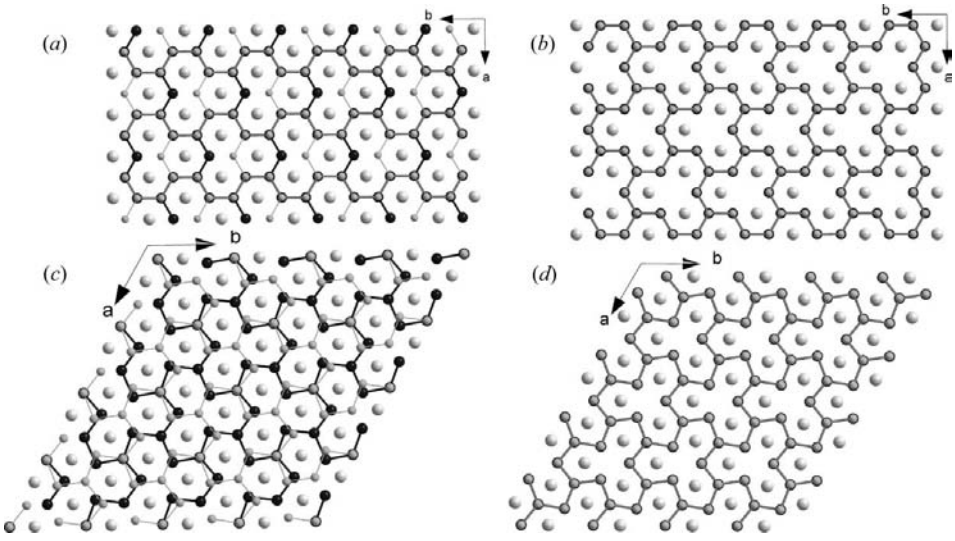

Figure 11
The (*a*) and (*b*) generated, and (*c*) and (*d*) observed structures of Y_3Ge_5 (*a*), (*c*) and Yb_3Ge_5 (*b*), (*d*). Adjacent layers of Ge are indicated with dark and light blue.

al. (1989) and Lee *et al.* (1992), with Figs. 1–3 and 5 in Lee *et al.* (1992) being particularly interesting.

7. Conclusions

We have successfully synthesized nine new compounds in the Er–Ge system. The compounds all adopt the AlB_2-type structure, but with long-range ordering of the vacancies in the 6^3 net formed by the Ge atoms. The structures are described as a family, using a (3 + 1)-dimensional approach. The derived model successfully describes the entire composition range $ErGe_2$ to Er_2Ge_3, with the exception of the Er_3Ge_5 line phase discussed in §6.

References

Arnaud d'Avitaya, F., Perio, A., Oberlin, J.-C., Campidelli, Y. & Chroboczek, J. A. (1989). *Appl. Phys. Lett.* **54**, 2198–2200.

Boulet, P., Bouëxière, D., Rebizant, J. & Wastin, F. (2001). *J. Solid State Chem.* **156**, 313–320.

Boulet, P., Bouëxière, D., Rebizant, J. & Wastin, F. (2003). *J. Alloys Compd.* **349**, 172–179.

Hoffmann, R.-D. & Pöttgen, R. (2001). *Z. Kristallogr.* **216**, 127–145.

Ijjaali, I., Venturini, G. & Malaman, B. (1999). *J. Alloys Compd.* **284**, 237–242.

Lee, T. L., Chen, L. J. & Chen, F. R. (1992). *J. Appl. Phys.* **71**, 3307–3312.

Mayer, I. P., Banks, E. & Post, B. (1962). *J. Phys. Chem.* **66**, 693–696.

Netzer, F. P. (1995). *J. Phys. Condens. Matter*, **7**, 991–1022.

Palenzona, A., Manfrinetti, P., Brutti, S. & Balducci, G. (2003). *J. Alloys Compd.* **348**, 100–104.

Perri, A., Binder, I. & Post, B. (1959). *J. Phys. Chem.* **63**, 616–619.

Petricek, V., Dusek, M. & Palatinus, L. (2000). *JANA*. Institute of Physics, Praha, Czech Republic.

Pöttgen, R., Hoffmann, R.-D. & Kußmann, D. (1998). *Z. Anorg. Allg. Chem.* **624**, 945–951.

Smith, G. S., Johnson, Q. & Tharp, A. G. (1965). *Acta Cryst.* **18**, 1085–1086.

Tharp, A. G. (1962). *J. Phys. Chem.* **66**, 758–760.

Venturini, G., Ijjaali, I. & Malaman, B. (1999*a*). *J. Alloys Compd.* **284**, 262–269.

Venturini, G., Ijjaali, I. & Malaman, B. (1999*b*). *J. Alloys Compd.* **289**, 116–119.

Zachariasen, W. H. (1949). *Acta Cryst.* **2**, 94–99.